Developmental Cell, Volume *57*

Supplemental information

γ-secretase promotes *Drosophila* postsynaptic development through the cleavage of a Wnt receptor

Lucas J. Restrepo, Alison T. DePew, Elizabeth R. Moese, Stephen R. Tymanskyj, Michael J. Parisi, Michael A. Aimino, Juan Carlos Duhart, Hong Fei, and Timothy J. Mosca

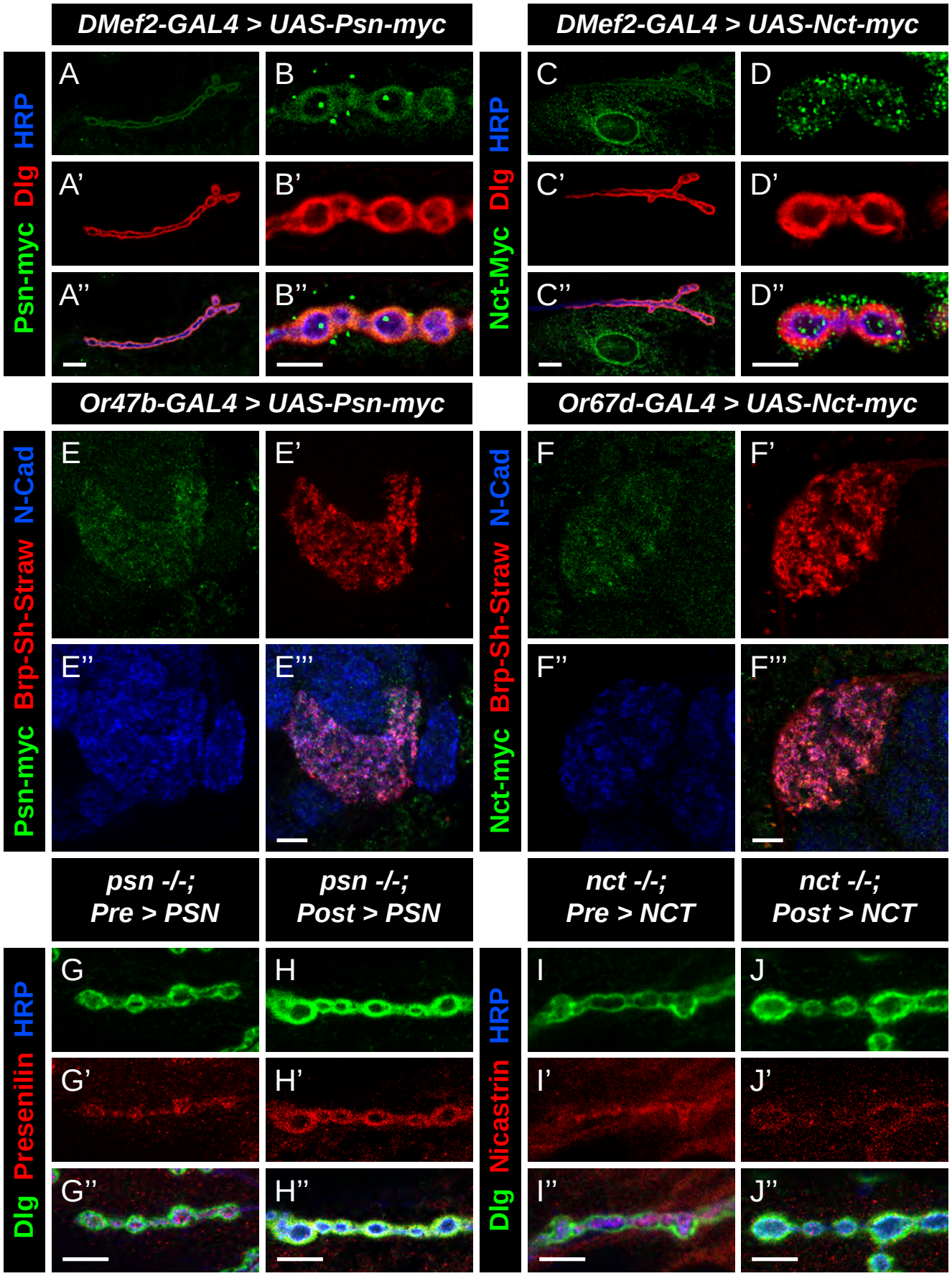
DMef2-GAL4 > UAS-Psn-myc
DMef2-GAL4 > UAS-Nct-myc
Psn-myc Dlg HRP
Nct-Myc Dlg HRP
A
B
C
D
A'
B'
C'
D'
A''
B''
C''
D''
Or47b-GAL4 > UAS-Psn-myc
Or67d-GAL4 > UAS-Nct-myc
Psn-myc Brp-Sh-Straw N-Cad
Nct-myc Brp-Sh-Straw N-Cad
E
E'
F
F'
E''
E'''
F''
F'''
psn -/-;
Pre > PSN
psn -/-;
Post > PSN
nct -/-;
Pre > NCT
nct -/-;
Post > NCT
Dlg Presenilin HRP
Dlg Nicastrin HRP
G
H
I
J
G'
H'
I'
J'
G''
H''
I''
J''

Figure S1, related to Figures 3 and 4. Epitope-tagged Presenilin and Nicastrin can localize to synaptic regions.

(A-D) Representative confocal images of larvae expressing Psn-myc (A-B) or Nct-myc (C-D) in muscles and stained with antibodies to Myc (green), Dlg (red), and HRP (blue). Exogenously expressed Psn and Nct can localize to the postsynaptic region, consistent with endogenous localization of each protein. High magnification images show an overlap with the largely postsynaptic marker Dlg (B,D). Note also that Nct-myc can also localize to the nuclear periphery (C-D), where Fz2 is cleaved to promote nuclear entry.

(E-F) Representative single confocal sections of adult brains expressing Psn-myc (E) or Nct-myc (F) and the active zone label Brp-Short in Or47b-positive olfactory receptor neurons that project to the VA1v glomerulus and stained with antibodies to Myc (green), Brp-Short (red), and N-Cadherin (blue). Both Psn-myc and Nct-myc can localize to the synapse-rich regions of these neurons, indicating synaptic localization in both the central and peripheral nervous systems of γ-secretase components.

(G-H) Representative single confocal sections of *psn* mutants expressing Presenilin in presynaptic motoneurons (G) or postsynaptic muscles (H) and stained with antibodies to endogenous Presenilin (red), Dlg (green), and HRP (blue). In these genotypes, the endogenous antibody recognizes the exogenously expressed Psn transgene, validating the tissue-specific transgene expression using endogenous Psn.

(I-J) Representative single confocal sections of *nct* mutants expressing Nicastrin in presynaptic motoneurons (G) or postsynaptic muscles (H) and stained with antibodies to endogenous Nicastrin (red), Dlg (green), and HRP (blue). In these genotypes, the endogenous antibody recognizes the exogenously expressed Nct transgene, validating the tissue-specific transgene expression using endogenous Nct.

Scale bar = 10 μm (A,C), 5 μm (B,D, G-J), or 20 μm (E-F).

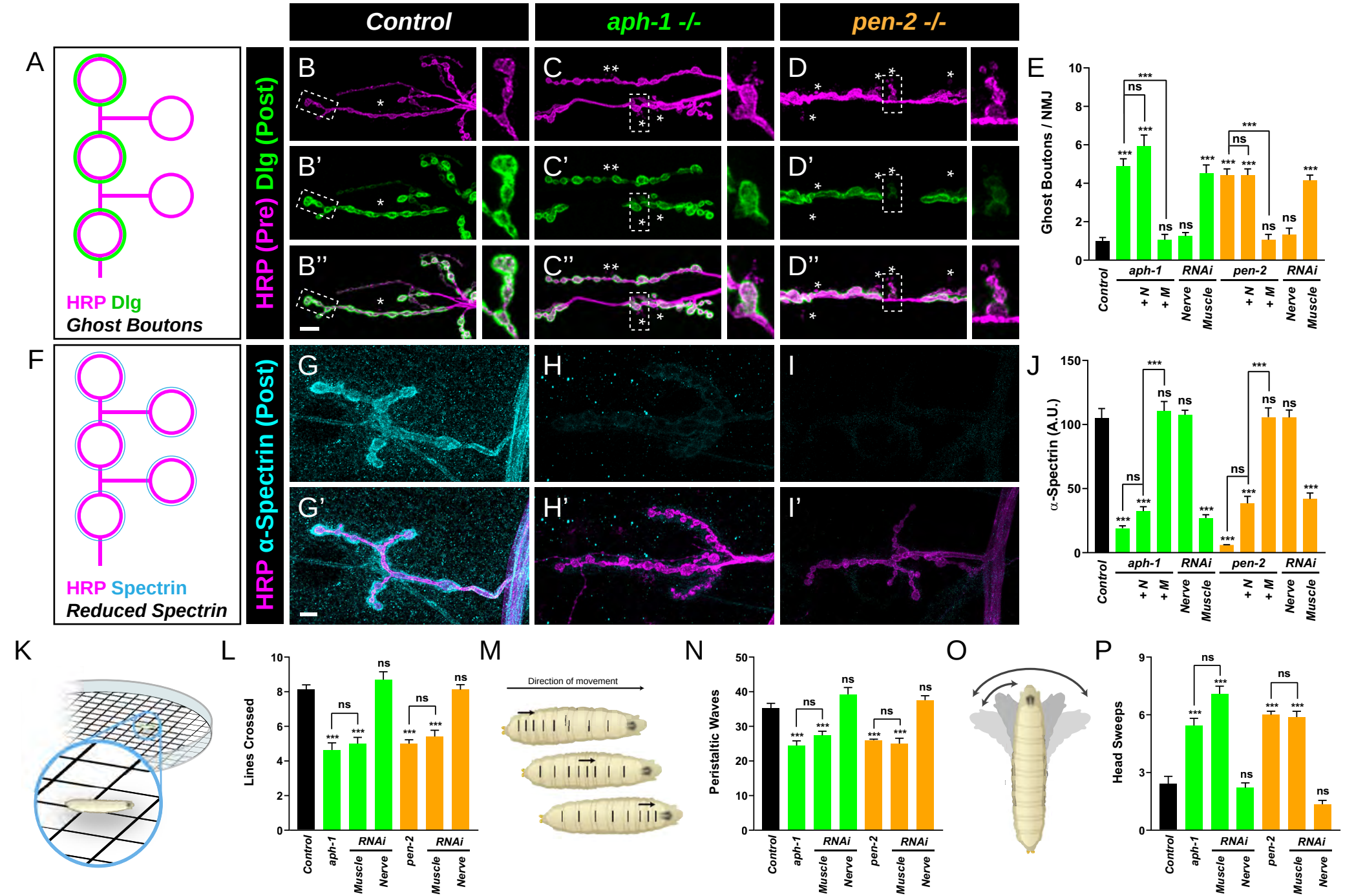
Control
aph-1 -/-
pen-2 -/-
A
HRP Dlg
Ghost Boutons
HRP (Pre) Dlg (Post)
B
B'
B''
C
C'
C''
D
D'
D''
E
Ghost Boutons / NMJ
Control
aph-1
RNAi
pen-2
RNAi
+ N
+ M
Nerve
Muscle
F
HRP Spectrin
Reduced Spectrin
HRP α-Spectrin (Post)
G
G'
H
H'
I
I'
J
α-Spectrin (A.U.)
K
L
Lines Crossed
M
Direction of movement
N
Peristaltic Waves
O
P
Head Sweeps

Figure S2, related to Figure 4. Loss of postsynaptic *aph-1* or *pen-2* impairs postsynaptic development and function.

(A) Schematic of the ghost bouton phenotype in maturation mutants. Normal boutons contain presynaptic HRP (magenta) staining and postsynaptic Dlg (green) staining while ghost boutons have only presynaptic HRP staining.

(B-D) Representative confocal images of control (B), *aph-1* mutant (C), and *pen-2* mutant (D) larvae stained with antibodies against HRP (magenta) and Dlg (green). Asterisks indicate ghost boutons and insets represent high magnification ghost or control boutons marked by the dashed line. *aph-1* and *pen-2* mutants show an increased incidence of ghost boutons, indicating impaired postsynaptic development and maturation.

(E) Quantification of ghost boutons in mutant, rescue, and RNAi genotypes. *aph-1* and *pen-2* mutants show a 5-fold increase in ghost boutons over control genotypes. The ghost bouton phenotype can be suppressed by postsynaptic muscle expression of Aph-1 or Pen-2 in the respective mutant (+ M) but not by presynaptic neuronal expression (+ N). Further, the phenotype is recapitulated by muscle (but not neuronal) *aph-1* or *pen-2* RNAi.

(F) Schematic of the reduced spectrin phenotype in maturation mutants: at all boutons, reduced thickness of spectrin staining and intensity indicates impaired maturation.

(G-I) Representative confocal images of control (G), *aph-1* mutant (H), and *pen-2* mutant (I) larvae stained with antibodies against HRP (magenta) and α-spectrin (cyan). α-spectrin fluorescence and thickness is markedly reduced (but not eliminated) in *aph-1* and *pen-2* mutants while HRP staining is unaffected.

(J) Quantification of α-spectrin fluorescence intensity in mutant, rescue, and RNAi genotypes. α-spectrin is reduced by 80% in *aph-1* and *pen-2* mutants; the α-spectrin phenotype is suppressed by muscle expression (+ M) but not neuronal expression (+ N), indicating a postsynaptic function for each in maturation and development. Similarly, muscle, but not neuronal, RNAi induces a comparable phenotype, as with *psn* and *nct*.

(K) Diagram of larval crawling assay to measure motility.

(L) Quantification of larval motility in mutant and RNAi genotypes. Loss of *aph-1* and *pen-2* impairs the number of lines crossed. In both mutants, the crawling deficit is recapitulated by muscle RNAi and not neuronal, indicating a postsynaptic role in larval motility.

(M) Diagram of larval peristaltic waves with arrows indicating direction of movement and lines on the larva denoting body wall segments.

(N) Quantification of peristaltic waves in mutant and RNAi genotypes. Loss of *aph-1* or *pen-2* reduces peristaltic wave number. The peristalsis defect is completely recapitulated in muscle RNAi of either gene but not by neuronal RNAi.

(O) Diagram of the larval head sweep. Arrows and shading indicate directions of motion during the head sweep behavior.

(P) Quantification of head sweeps in mutant and RNAi behavior. Both *aph-1* and *pen-2* mutants show an increase in head sweeps over control larvae. This behavioral phenotype is recapitulated again by muscle, and not neuronal RNAi. Taken together, the data suggests that postsynaptic *aph-1* and *pen-2* are essential to promote normal postsynaptic morphology, maturation, and larval behavior.

For all experiments, the data represent mean ± SEM with significance calculated by ANOVA followed by a Tukey's test for multiple comparisons. For morphological experiments, $n \geq 8$ larvae, 16 NMJs. For behavioral experiments, $n \geq 24$ larvae. **, $p < 0.01$, ***, $p < 0.001$, n.s. = not significant. Scale bar = 10 μm, 5 μm for insets.

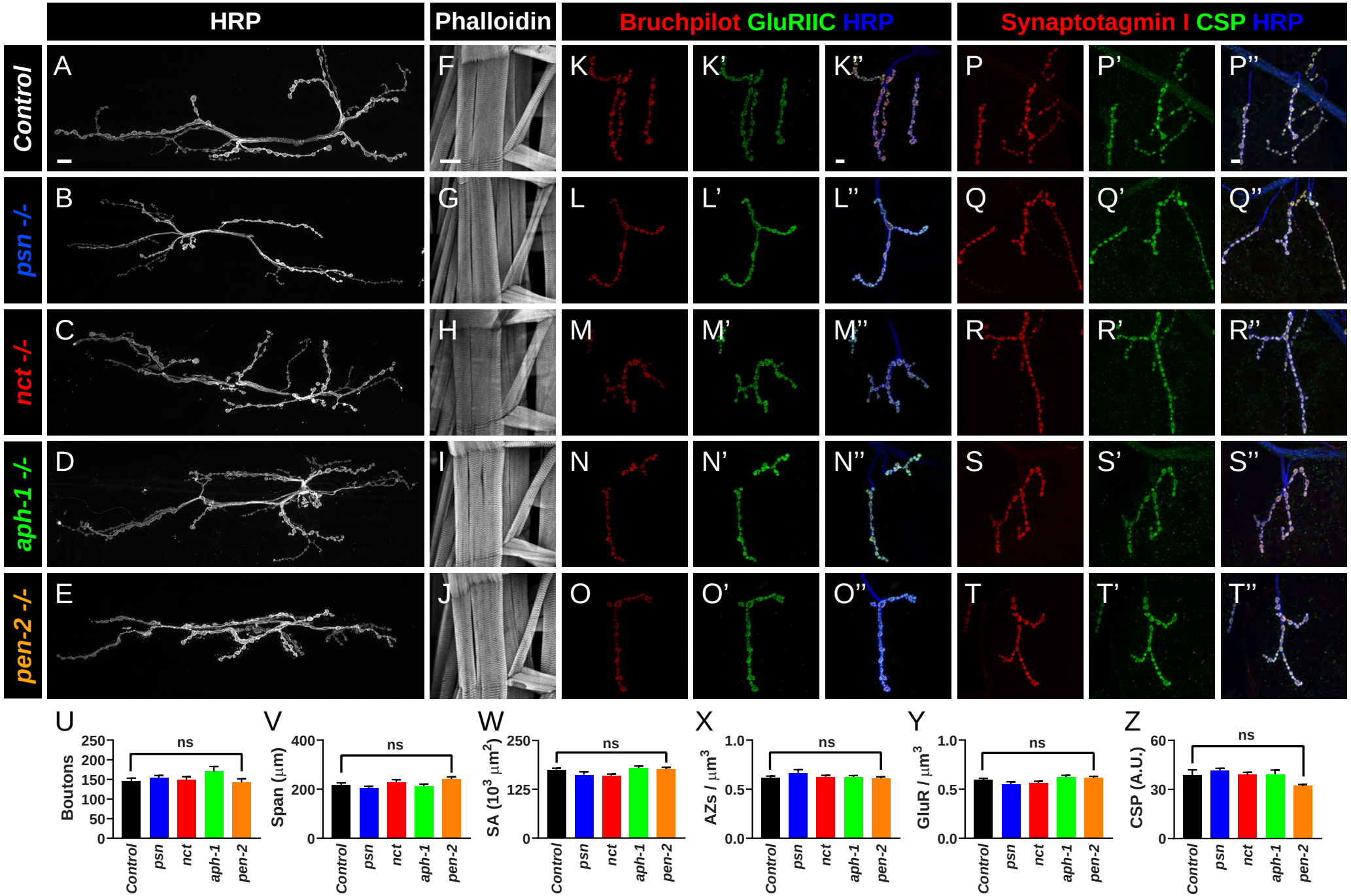
HRP
Phalloidin
Bruchpilot GluRIIC HRP
Synaptotagmin I CSP HRP
Control
psn -/-
nct -/-
aph-1 -/-
pen-2 -/-
A
B
C
D
E
F
G
H
I
J
K
K'
K''
L
L'
L''
M
M'
M''
N
N'
N''
O
O'
O''
P
P'
P''
Q
Q'
Q''
R
R'
R''
S
S'
S''
T
T'
T''
U
Boutons
250
200
150
100
50
0
ns
Control
psn
nct
aph-1
pen-2
V
Span (μm)
400
200
0
ns
W
SA (10³ μm²)
250
125
0
ns
X
AZs / μm³
1.0
0.5
0.0
ns
Y
GluR / μm³
1.0
0.5
0.0
ns
Z
CSP (A.U.)
60
30
0
ns

Figure S3, related to Figure 4. γ-secretase mutants show otherwise normal synaptic development.

(A-E) Representative NMJs at muscle 6/7 stained with antibodies to HRP in control (A), *psn* mutant (B), *nct* mutant (C), *aph-1* mutant (D), and *pen-2* mutant (E) larvae.

(F-J), Representative images of the larval body wall muscle field containing muscles 6, 7, 12, 13, 5, 8, and 4 stained with TexasRed-conjugated phalloidin in control (F), *psn* mutant (G), *nct* mutant (H), *aph-1* mutant (I), and *pen-2* mutant (J) larvae.

(K-O) Representative NMJs at muscle 4 stained with antibodies to Bruchpilot (red), GluRIIC (green), and HRP (blue) in control (K), *psn* mutant (L), *nct* mutant (M), *aph-1* mutant (N), and *pen-2* mutant (O) larvae.

(P-T) Representative NMJs at muscle 4 stained with antibodies to Synaptotagmin I (red), CSP (green), and HRP (blue) in control (P), *psn* mutant (Q), *nct* mutant (R), *aph-1* mutant (S), and *pen-2* mutant (T) larvae. In all cases, each mutant parameter appears similar to control larvae, suggesting no defects in generalized synaptic development.

(U-Z) Quantification of bouton number (U), NMJ length / synaptic span (V), muscle surface area (W), active zone density (X), glutamate receptor density (Y), and CSP fluorescence (Z) in all genotypes. No quantitative differences or phenotypes were observed in any of the γ-secretase subunit mutants. This data indicates that defects in postsynaptic development and maturation are unlikely to be secondary to gross defects in synapse formation and organization.

For all experiments, the data represent mean ± SEM with statistical significance calculated by ANOVA followed by a Tukey's test for multiple comparisons. In all cases, $n \geq 6$ larvae, 12 NMJs. n.s. = not significant. SA = surface area. AZs = active zones. GluR = glutamate receptor. Scale bar = 10 μm (a-e, k-t) or 100 μm (f-j).

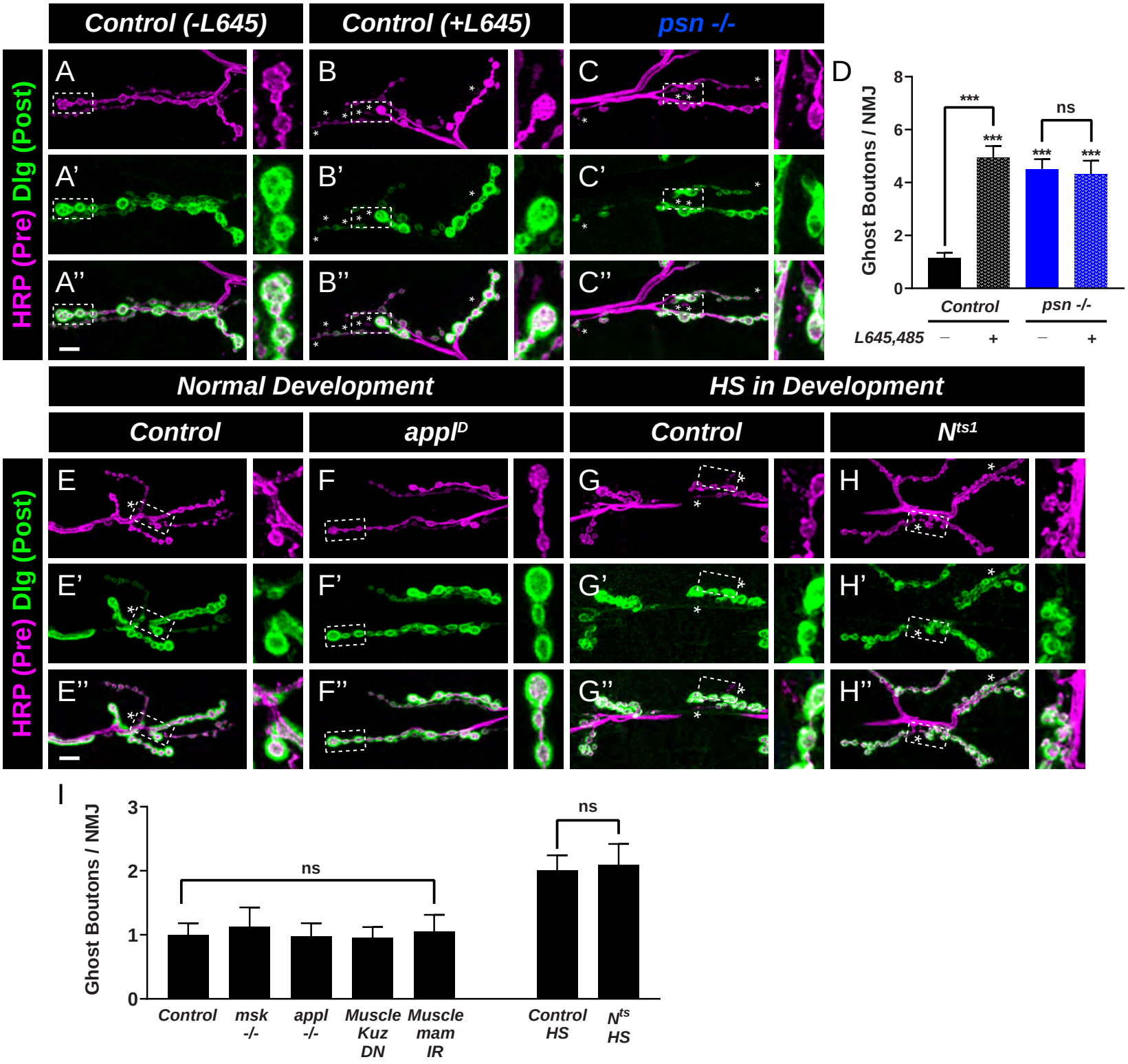
Control (-L645)
Control (+L645)
psn -/-
HRP (Pre) Dlg (Post)
A
A'
A''
B
B'
B''
C
C'
C''
D
Ghost Boutons / NMJ
***
ns
Control
psn -/-
L645,485
Normal Development
HS in Development
Control
applD
Control
Nts1
E
E'
E''
F
F'
F''
G
G'
G''
H
H'
H''
I
Ghost Boutons / NMJ
ns
ns
Control
msk -/-
appl -/-
Muscle Kuz DN
Muscle mam IR
Control HS
Nts HS

Figure S4, related to Figures 4 and 5. Pharmacological blockade of y-secretase activity in *Drosophila* impairs postsynaptic development while the Notch pathway is dispensable for postsynaptic maturation.

(A-C) Representative confocal images of non-drug treated (A) and drug-treated (B) control or *psn* mutant (C) larvae stained with antibodies for HRP (magenta) and Dlg (green). Asterisks indicate ghost boutons. Insets represent high magnification ghost or control boutons marked by the dashed line. Larvae reared on L685,458 show increased ghost boutons.

(D) Quantification of ghost boutons. Rearing on L685,458 causes a 5-fold increase in ghost boutons in otherwise-wild-type larvae. This change is not observed in *psn* mutants, suggesting that these do not enhance each other and likely target the same pathway.

(E-H) Representative confocal images of NMJs in control (E, G), *appl* mutant (F) and *Notch* mutant (H) larvae and stained with antibodies to HRP (magenta) and Dlg (green). Loss of *appl*, which interacts with the Notch pathway, does not show an increase in ghost boutons. Developmental reduction of Notch itself also does not show an increase in ghost boutons over control larvae. *Control* and N^{TS1} larvae for this experiment were raised at a higher temperature (29°C) during development (HS in Development = heat-shocked during development), accounting for the increase in ghost boutons when compared to controls raised at 25°C. Insets represent high magnification ghost or control boutons marked by the dashed line.

(I) Quantification of ghost boutons. In multiple mutants in components of the Notch pathway or muscle-specific perturbation of Notch pathway components, no increases in ghost boutons were observed. This data indicates that perturbing the Notch pathway has no effect on postsynaptic development and maturation, suggesting that γ-secretase does not function through Notch to mediate synaptic maturation.

For all experiments, the data represent mean ± SEM with statistical significance calculated by ANOVA followed by a Tukey's test for multiple comparisons. For (A-D), $n \geq 8$ larvae, 15 NMJs. For (E – I), $n \geq 5$ larvae, 10 NMJs. ***, $p < 0.001$, n.s. = not significant. Scale bar = 10 μm, 5 μm for insets.

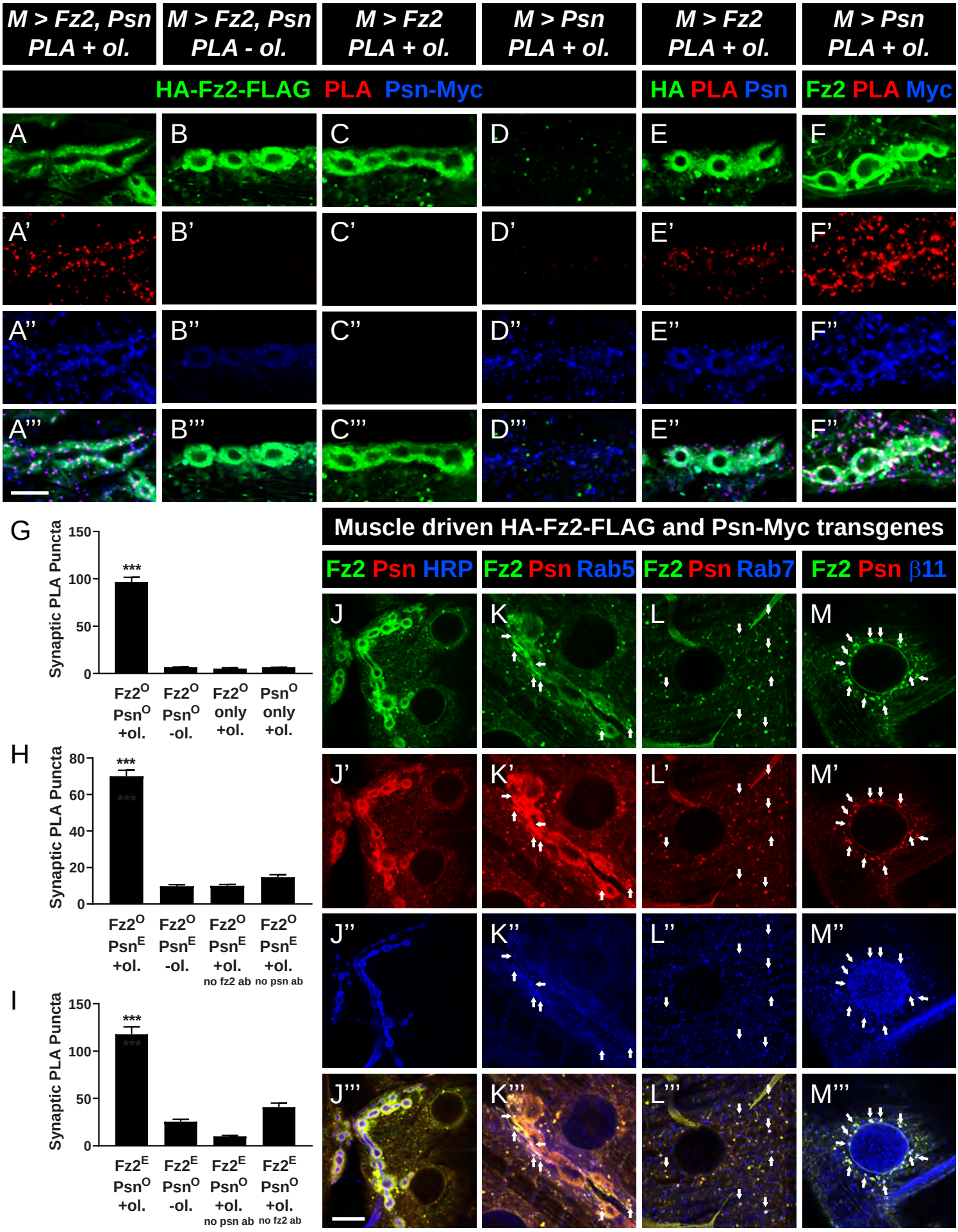
M > Fz2, Psn PLA + ol.
M > Fz2, Psn PLA - ol.
M > Fz2 PLA + ol.
M > Psn PLA + ol.
M > Fz2 PLA + ol.
M > Psn PLA + ol.
HA-Fz2-FLAG PLA Psn-Myc
HA PLA Psn
Fz2 PLA Myc
A
B
C
D
E
F
A'
B'
C'
D'
E'
F'
A''
B''
C''
D''
E''
F''
A'''
B'''
C'''
D'''
E''
F''
G
Synaptic PLA Puncta
150
100
50
0
***
Fz2O PsnO +ol.
Fz2O PsnO -ol.
Fz2O only +ol.
PsnO only +ol.
H
Synaptic PLA Puncta
80
60
40
20
0
***
***
Fz2O PsnE +ol.
Fz2O PsnE -ol.
Fz2O PsnE +ol. no fz2 ab
Fz2O PsnE +ol. no psn ab
I
Synaptic PLA Puncta
150
100
50
0
***
***
Fz2E PsnO +ol.
Fz2E PsnO -ol.
Fz2E PsnO +ol. no psn ab
Fz2E PsnO +ol. no fz2 ab
Muscle driven HA-Fz2-FLAG and Psn-Myc transgenes
Fz2 Psn HRP
Fz2 Psn Rab5
Fz2 Psn Rab7
Fz2 Psn β11
J
K
L
M
J'
K'
L'
M'
J''
K''
L''
M''
J'''
K'''
L'''
M'''

Figure S5, related to Figure 5. Epitope-tagged Fz2 and Presenilin co-localize to synapses and subcellular compartments consistent with their shared trafficking.

(A-D) Representative confocal micrographs of larvae expressing HA-Fz2-FLAG and Psn-Myc in postsynaptic muscles (A-B), HA-Fz2-FLAG only (C), or Psn-Myc only (D) stained for antibodies to FLAG (green) and Myc (blue) and reacted with a proximity ligation assay (red). Positive PLA signal was observed when both transgenes were present and the oligo reaction conducted (A); no PLA signal was observed above background when the oligo reaction was omitted (B) or only one transgene was expressed (C-D).
(E) Representative confocal micrographs of larvae expressing HA-Fz2-FLAG in postsynaptic muscles and stained for antibodies to HA (green) and endogenous Psn (blue) and reacted with a proximity ligation assay (red). Positive synaptic PLA signal was observed, suggesting exogenously expressed Fz2 and endogenous Psn are within 40 nm of each other. Some signal was seen extrasynaptically, which may indicate trafficking.
(F) Representative confocal micrographs of larvae expressing Psn-Myc in postsynaptic muscles and stained for antibodies to endogenous Fz2 (green) and Myc (blue) and reacted with a proximity ligation assay (red). Positive PLA signal was observed at the synapse, suggesting exogenously expressed Psn and endogenous Fz2 are within 40 nm of each other. Signal was also observed extrasynaptically, which may indicate trafficking.
(G) Quantification of PLA puncta in representative experiments expressing HA-Fz2-FLAG ($Fz2^{O}$) and Psn-Myc (Psn^{O}) in muscles. When both constructs are expressed and the oligo reaction done ($Fz2^{O}$ Psn^{O} +ol.), a significant increase in synaptic PLA puncta over background is seen. When the oligo is removed ($Fz2^{O}$ Psn^{O} -ol.) or only Fz2 ($Fz2^{O}$ only +ol.) or Psn (Psn^{O} only +ol.) is expressed, few puncta are seen, indicating no interaction.
(H) Quantification of PLA puncta in representative experiments expressing HA-Fz2-FLAG in muscles ($Fz2^{O}$) and examining interaction with endogenous Psn (Psn^{E}). When both antibodies are utilized and the oligo reaction conducted ($Fz2^{O}$ Psn^{E} +ol.), a significant increase in synaptic PLA puncta over background is observed. When the oligo reaction is removed ($Fz2^{O}$ Psn^{E} -ol.) or the Fz2 ($Fz2^{O}$ Psn^{E} +ol. no fz2 ab) or Psn antibody are omitted ($Fz2^{O}$ Psn^{E} +ol. no psn ab), few puncta are observed indicating no interaction.
(I) Quantification of PLA puncta in representative experiments expressing Psn-myc in muscles (Psn^{O}) and examining interaction with endogenous Fz2 ($Fz2^{E}$). When both antibodies are utilized and the oligo reaction conducted ($Fz2^{E}$ Psn^{O} +ol.), a significant increase in synaptic PLA puncta over background is observed. When the oligo reaction is removed ($Fz2^{E}$ Psn^{O} -ol.) or the Psn ($Fz2^{E}$ Psn^{O} +ol. no psn ab) or Fz2 antibody are omitted ($Fz2^{E}$ Psn^{O} +ol. no fz2 ab), few puncta are observed indicating no interaction.
(J-M) Representative confocal images of *Drosophila* larvae expressing HA-Fz2-FLAG and Psn-Myc in postsynaptic muscles and stained with antibodies to Fz2 (green, HA), Psn (red, Myc), or other cellular markers (blue, HRP in J; Rab5 in K; Rab7 in L; Importin-β11 in M). Fz2 and Psn colocalize at postsynaptic regions and the nuclear periphery as well as in puncta throughout the muscle (J). Near the synapse, they colocalize with the early endosome marker Rab5 (K) and near nuclei with the late endosome marker Rab7 (L) and the nuclear import factor Importin-β11 (M). This is consistent with known subcellular compartmentalization of Fz2 and suggests shared trafficking. For (A-I), n ≥ 3 larvae per experiment, 4 NMJs per larvae. Scale bar = 5 μm for (A-F), 10 μm for (J-M). ***, $p < 0.001$.

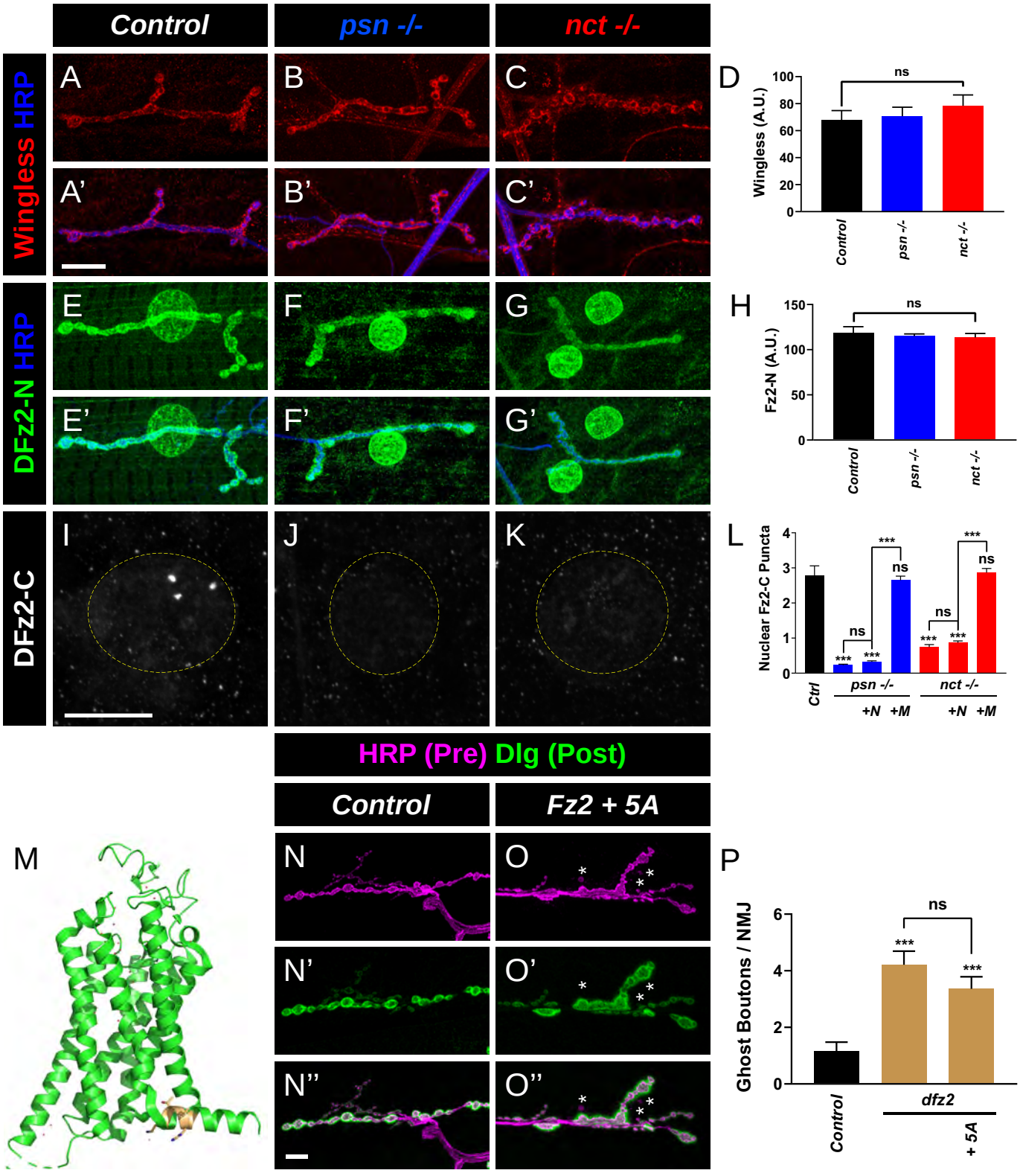
Control
psn -/-
nct -/-
Wingless HRP
DFz2-N HRP
DFz2-C
A
A'
B
B'
C
C'
D
Wingless (A.U.)
ns
Control
psn -/-
nct -/-
E
E'
F
F'
G
G'
H
Fz2-N (A.U.)
I
J
K
L
Nuclear Fz2-C Puncta
Ctrl
+N
+M
HRP (Pre) Dlg (Post)
Fz2 + 5A
M
N
N'
N''
O
O'
O''
P
Ghost Boutons / NMJ
dfz2
+ 5A

Figure S6, related to Figure 5. Examination of Wnt pathway steps in *psn* and *nct* mutants and Fz2 cleavage site manipulation in promoting postsynaptic development.

(A-C) Representative confocal images of control (A), *psn* mutant (B), and *nct* mutant (C) larvae stained with antibodies to the Wnt ligand, Wingless (red) and HRP (blue). Wingless properly localizes to the NMJ in all mutants observed, suggesting that expression failure cannot account for the observed maturation defects.

(D) Quantification of Wingless fluorescence. No significant differences in levels are observed in *psn* and *nct* mutants.

(E-G) Representative confocal images of control (D), *psn* mutant (E), and *nct* mutant (F) larvae stained with antibodies to the N-terminus of Fz2 (Fz2-N, green) and HRP (blue). Fz2-N properly localizes to the NMJ in all mutants observed, suggesting that expression failure cannot account for the observed maturation defects. Fz2-N also decorates the nuclear envelope, further indicating that the endocytosis and trafficking of Fz2 (Ataman et al., 2006; Mathew et al., 2005) is not perturbed in *psn* and *nct* mutants.

(H) Quantification of Fz2-N fluorescence. No significant differences in the levels of Fz2-N staining are observed in *psn* and *nct* mutants.

(I-K) Representative confocal images of control (I), *psn* mutant (J), and *nct* mutant (K) larvae stained with antibodies to Fz2-C. The nuclear border is outlined (dashed lines). All mutants lack nuclear Fz2-C staining, indicating a failure of Fz2-C to enter the nucleus or be cleaved.

(L) Quantification of Fz2-C puncta in mutant and rescue genotypes. Loss of *psn* or *nct* decreases nuclear Fz2-C puncta by 85-93%. The Fz2-C nuclear defect can be suppressed by muscle expression of the respective transgene but not neuronal expression. This indicates that postsynaptic γ-secretase is required for nuclear Fz2-C entry.

(M) Structural model of *Drosophila* Fz2 based on the human Fz4 crystal structure. The KTLES cleavage site is indicated in yellow. The site is located immediately following the TM domain.

(N-O) Representative confocal images of control larvae (B) or *dfz2* mutant larvae expressing Fz2 with 5 alanine residues inserted between the last transmembrane domain and the KTLES site in the postsynaptic muscles (C) and stained with antibodies to HRP (magenta) and Dlg (green). Asterisks indicate ghost boutons.

(P) Quantification of ghost boutons. Expression of Fz2 with an intact, but shifted, cleavage site, fails to rescue the *dfz2* mutant phenotype, suggesting that the position of the cleavage site proximal to the membrane is essential for normal function. Increasing the distance between the membrane and the cleavage site impairs the ability of Fz2 to promote postsynaptic development.

For all experiments, the data represent mean ± SEM with statistical significance calculated by ANOVA followed by a Tukey's test for multiple comparisons. For (A-H), $n \geq 5$ larvae, 9 NMJs. For (I-L), $n \geq 6$ larvae, 12 NMJs. For (N-P), $n \geq 6$ larvae, 11 NMJs.

***, $p < 0.001$. n.s. = not significant. Scale bar = 10 μm (A-H, N-O) or 5 μm (I-K).

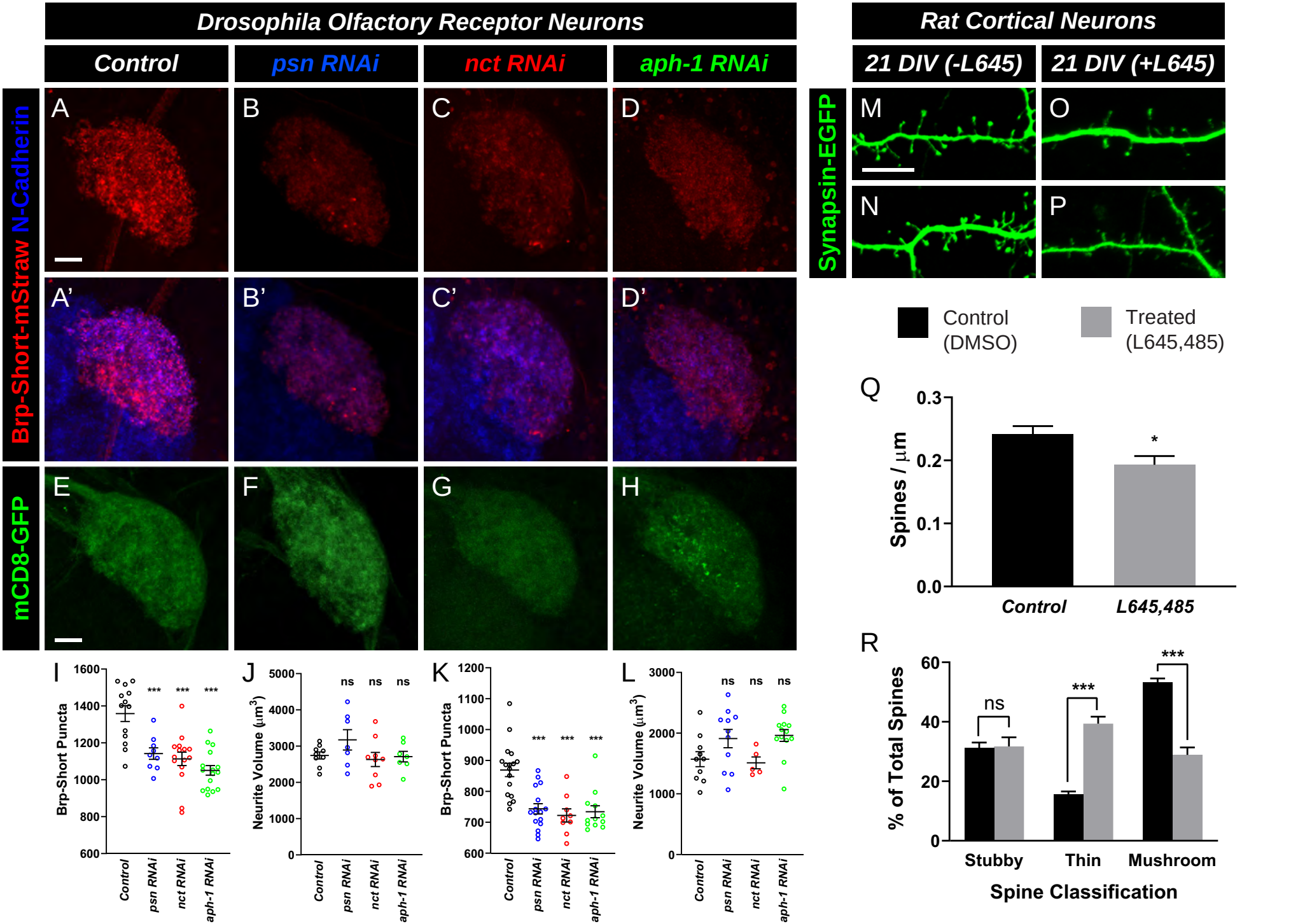
Drosophila Olfactory Receptor Neurons
Control
psn RNAi
nct RNAi
aph-1 RNAi
Brp-Short-mStraw N-Cadherin
mCD8-GFP
A
B
C
D
A'
B'
C'
D'
E
F
G
H
I
Brp-Short Puncta
J
Neurite Volume (µm3)
K
Brp-Short Puncta
L
Neurite Volume (µm3)
ns
***
Rat Cortical Neurons
21 DIV (-L645)
21 DIV (+L645)
Synapsin-EGFP
M
N
O
P
Control (DMSO)
Treated (L645,485)
Q
Spines / µm
*
Control
L645,485
R
% of Total Spines
Stubby
Thin
Mushroom
Spine Classification

Figure S7, related to STAR Methods. Loss of γ-secretase subunits in olfactory receptor neurons or pharmacologically inhibiting γ-secretase activity blockade in primary mammalian neurons impairs central neuron synaptic development.

(A-D) Representative high magnification confocal stack images of DA1 olfactory receptor neuron (ORN) axon terminals in the DA1 glomerulus of male adult *Drosophila* expressing Brp-Short-mStraw and stained with antibodies against mStraw (red) and N-Cadherin (blue). RNAi against *psn* (B), *nct* (C), or *aph-1* (D) all show fewer Brp-Short-mStraw puncta compared to control animals (A).

(E-H) Representative high magnification confocal stack images of DA1 olfactory receptor neuron (ORN) axon terminals in the DA1 glomerulus of male adult *Drosophila* expressing mCD8-GFP and stained with antibodies against GFP (green) and N-Cadherin (blue). RNAi against *psn* (F), *nct* (G), or *aph-1* (H) do not visibly alter GFP staining from control animals (E).

(I,K) Quantification of Brp-Short-mStraw puncta in DA1 ORNs of male (I) and female (K) flies. There is an 18-27% reduction in Brp-Short-mStraw puncta when γ-secretase subunits are perturbed.

(J,L) Quantification of mCD8-GFP rendered neurite volume in DA1 ORNs of male (J) and female (L) flies. There are no changes in the neurite volume regardless of genetic perturbation, suggesting that while growth is unaffected, the achievement of a mature number of Brp-Short-mStraw puncta is impaired. This data indicates that γ-secretase in involved in central neuron development in *Drosophila*.

(M-N) High magnification of dendritic spines on 21 DIV mammalian primary neuron cultures not treated with L685,458 and stained with antibodies to GFP (green).

(O-P) 21 DIV cultures stained as above but treated with L685,458. Though dendritic spines are still visible, the mushroom-headed spines in control samples are not often visible; instead, there are more filopodial-like spines.

(Q) Quantification of dendritic spine density. There is a modest reduction in spine density when γ-secretase activity is perturbed, consistent with previous work (Inoue et al., 2009; Javier-Torrent et al., 2019).

(R) Quantification of dendritic spine type. Treated samples show an increase in thin, filopodial outgrowth and a concomitant reduction in mature, mushroom-headed spines. This data indicates that mammalian dendritic development is also impaired by blocking γ-secretase activity, consistent with a conserved role.

For all experiments, the data represent mean ± SEM with statistical significance calculated by ANOVA followed by a Tukey's test for multiple comparisons. In (A-L), $n \geq 5$ brains, 9 glomeruli. In (M-R), $n \geq 200$ spines from 10 neurons. ***, $p < 0.001$, n.s. = not significant. Scale bar (A-H) = 20 μm or 10 μm (M-P).

Table S1, related to Figure 2. Screen for Protease Genes Involved in Synaptic Maturation.

List of genes examined in our screen (Figure 2) for protease genes involved in synaptic maturation. Genes are listed alphabetically and the blinded number in the screen is indicated as is the VDRC or Harvard TRiP collection stock number followed by the number of ghost or footprint boutons listed as mean ± SEM (*n*). * Line from Harvard TRiP Collection

Gene	Screen Line	RNAi Line (s)	Ghosts				Footprints			
			Mean	±	SEM	(*n*)	Mean	±	SEM	(*n*)
Acer	1	1187	1.02	±	0.13	(*30*)	0.06	±	0.06	(*16*)
AdamTS-A	11	3002, 102087	1.31	±	0.12	(*30*)	0.06	±	0.06	(*16*)
AdamTS-B	22	114135, 108644	0.99	±	0.16	(*30*)	0.00	±	0.00	(*16*)
CG10280	32	5733, 101800	1.17	±	0.13	(*30*)	0.06	±	0.06	(*16*)
CG10477	2	111082, 6029	1.07	±	0.14	(*30*)	0.00	±	0.00	(*16*)
CG10588	4	7030, 111057	1.17	±	0.21	(*30*)	0.06	±	0.06	(*16*)
CG11396	5	7285, 100912	1.07	±	0.18	(*41*)	0.00	±	0.00	(*16*)
CG11771	6	6258, 105164	1.33	±	0.12	(*30*)	0.00	±	0.00	(*16*)
CG11865	14	5112, 106934	0.89	±	0.16	(*30*)	0.00	±	0.00	(*16*)
CG14231	8	108695	0.98	±	0.18	(*30*)	0.06	±	0.06	(*16*)
CG15253	9	105983	1.39	±	0.40	(*23*)	0.13	±	0.13	(*16*)
CG15254	10	5110, 106542	0.90	±	0.13	(*30*)	0.00	±	0.00	(*16*)
CG15255	12	5402	1.03	±	0.16	(*30*)	0.00	±	0.00	(*16*)
CG2528	13	107208, 9786	1.60	±	0.19	(*30*)	0.00	±	0.00	(*16*)
CG3107	15	102698, 10154	1.19	±	0.17	(*30*)	0.00	±	0.00	(*16*)
CG5131	16	11548, 100257	1.09	±	0.16	(*30*)	0.06	±	0.06	(*16*)
CG5355	17	11622, 100768	1.21	±	0.18	(*30*)	0.00	±	0.00	(*16*)
CG5715	18	6250	1.26	±	0.21	(*30*)	0.00	±	0.00	(*16*)
CG6168	19	12811	1.45	±	0.17	(*47*)	0.06	±	0.06	(*16*)
CG6512	20	3606, 101663	1.12	±	0.18	(*30*)	0.00	±	0.00	(*16*)
CG6696	21	12822, 109175	1.02	±	0.15	(*30*)	0.06	±	0.06	(*16*)
CG6763	23	6243, 104986	1.38	±	0.21	(*30*)	0.00	±	0.00	(*16*)
CG6974	24	5663, 105294	1.22	±	0.21	(*30*)	0.06	±	0.06	(*16*)
CG7573	25	2419, 103153	1.66	±	0.20	(*30*)	0.00	±	0.00	(*16*)
CG7631	26	5113, 105010	1.46	±	0.29	(*30*)	0.00	±	0.00	(*16*)
CG7791	28	12285, 102289	1.14	±	0.18	(*30*)	0.00	±	0.00	(*16*)
CG8728	29	14012, 16436	1.00	±	0.15	(*30*)	0.00	±	0.00	(*16*)
CG9631	30	13221, 105550	1.05	±	0.14	(*30*)	0.00	±	0.00	(*16*)
CG9649	31	1321, 104575	1.03	±	0.12	(*30*)	0.00	±	0.00	(*16*)
Control	82	N/A	0.82	±	0.12	(*30*)	0.00	±	0.00	(*16*)
CSN5	96	JF03159*	1.01	±	0.17	(*30*)	0.00	±	0.00	(*16*)

Dredd	33	110428, 12252	1.15	±	0.09	(*30*)	0.00	±	0.00	(*16*)
Dronc	34	12376, 104278	1.21	±	0.12	(*30*)	0.00	±	0.00	(*16*)
frma	35	109584	1.16	±	0.13	(*30*)	0.06	±	0.06	(*16*)
Fz2	3	44390, 108998	3.50	±	0.30	(*30*)	0.00	±	0.00	(*16*)
goe	36	1174, 104608	1.05	±	0.14	(*30*)	0.00	±	0.00	(*16*)
Ide	37	6073, 107536	1.10	±	0.17	(*30*)	0.00	±	0.00	(*16*)
Invadolysin	38	5576	1.30	±	0.16	(*30*)	0.00	±	0.00	(*16*)
Jon25Bi	39	5245, 111014	1.06	±	0.13	(*30*)	0.06	±	0.06	(*16*)
Jon25Biii	40	17851, 111515	1.40	±	0.17	(*48*)	0.00	±	0.00	(*16*)
Jon65Aiii	41	6033, 112736	0.93	±	0.11	(*30*)	0.00	±	0.00	(*16*)
Jon66Ci	42	17527, 113078	1.22	±	0.14	(*30*)	0.06	±	0.06	(*16*)
Jon99Ci	43	6342, 106885	1.06	±	0.15	(*30*)	0.00	±	0.00	(*16*)
Jon99Fii	44	17783	1.26	±	0.17	(*30*)	0.00	±	0.00	(*16*)
Kul	45	12729, 105893	1.10	±	0.13	(*30*)	0.00	±	0.00	(*16*)
kuz	46	330255	1.07	±	0.12	(*30*)	0.00	±	0.00	(*16*)
loh	47	5502	1.12	±	0.14	(*30*)	0.06	±	0.06	(*16*)
Meltrin	48	2620, 110487	0.97	±	0.12	(*30*)	0.00	±	0.00	(*16*)
mmd	50	110577	1.02	±	0.12	(*30*)	0.00	±	0.00	(*16*)
Mmp1	51	108894, 330331	1.23	±	0.19	(*44*)	0.06	±	0.06	(*16*)
Mmp2	52	330203, 104713	1.24	±	0.16	(*41*)	0.00	±	0.00	(*16*)
MP1	53	5141, 107262	1.03	±	0.15	(*30*)	0.00	±	0.00	(*16*)
nct	49	JF02648*	5.02	±	0.42	(*42*)	0.00	±	0.00	(*16*)
Nrd1	54	9705, 102064	1.28	±	0.15	(*30*)	0.13	±	0.13	(*16*)
Ppn	55	6325, 101228	1.15	±	0.15	(*30*)	0.00	±	0.00	(*16*)
ProsA2	56	15087, 109089	1.18	±	0.12	(*30*)	0.00	±	0.00	(*16*)
ProsA3	57	108002	0.94	±	0.14	(*30*)	0.00	±	0.00	(*16*)
ProsA3T	58	106317, 9358	1.14	±	0.12	(*30*)	0.00	±	0.00	(*16*)
ProsA4	59	10962, 108682	1.11	±	0.16	(*30*)	0.00	±	0.00	(*16*)
ProsA4T1	60	107132, 17186	1.01	±	0.14	(*30*)	0.00	±	0.00	(*16*)
ProsA4T2	61	11356, 110303	0.81	±	0.15	(*30*)	0.19	±	0.14	(*16*)
ProsA5	62	7134, 108214	1.45	±	0.15	(*30*)	0.00	±	0.00	(*16*)
ProsA6	63	11466, 107987	0.85	±	0.17	(*30*)	0.00	±	0.00	(*16*)
ProsA6T	64	11719	1.16	±	0.18	(*30*)	0.13	±	0.13	(*16*)
ProsA7	65	3491, 109262	1.20	±	0.12	(*30*)	0.00	±	0.00	(*16*)
ProsB1	66	13913	0.98	±	0.14	(*30*)	0.00	±	0.00	(*16*)
ProsB2	67	10938, 101430	0.86	±	0.14	(*30*)	0.00	±	0.00	(*16*)
ProsB2R1	68	106009, 9563	1.03	±	0.17	(*30*)	0.00	±	0.00	(*16*)
ProsB2R2	69	7509, 112887	1.01	±	0.16	(*30*)	0.00	±	0.00	(*16*)
ProsB3	70	7449, 108041	1.00	±	0.17	(*30*)	0.06	±	0.06	(*16*)
ProsB4	71	8601	1.18	±	0.18	(*30*)	0.00	±	0.00	(*16*)
ProsB4R1	72	9343	1.06	±	0.15	(*30*)	0.00	±	0.00	(*16*)

ProsB4R2	73	105973, 9344	0.89	±	0.13	(*30*)	0.00	±	0.00	(*16*)
ProsB5	74	7568, 101404	1.01	±	0.17	(*30*)	0.00	±	0.00	(*16*)
ProsB5R1	75	105592, 14707	1.04	±	0.15	(*30*)	0.06	±	0.06	(*16*)
ProsB5R2	76	105262	1.18	±	0.15	(*30*)	0.00	±	0.00	(*16*)
ProsB6	77	105673	1.10	±	0.15	(*30*)	0.00	±	0.00	(*16*)
ProsB7	78	7457, 108365	1.14	±	0.16	(*30*)	0.00	±	0.00	(*16*)
psn	27	4624, 109329	2.93	±	0.29	(*44*)	0.00	±	0.00	(*16*)
rho-7	79	3775, 107598	1.07	±	0.20	(*30*)	0.00	±	0.00	(*16*)
S2P	80	1939, 102025	0.85	±	0.14	(*30*)	0.06	±	0.06	(*16*)
Semp1	81	5403, 103840	0.90	±	0.15	(*30*)	0.00	±	0.00	(*16*)
sona	83	110685	1.02	±	0.16	(*30*)	0.00	±	0.00	(*16*)
spg7	95	JF01565*	0.88	±	0.13	(*30*)	0.00	±	0.00	(*16*)
ste24a	84	2046, 101810	0.95	±	0.18	(*30*)	0.00	±	0.00	(*16*)
ste24b	85	105056, 2045	0.97	±	0.15	(*30*)	0.13	±	0.13	(*16*)
ste24c	94	49812	0.98	±	0.17	(*30*)	0.06	±	0.06	(*16*)
stl	86	2160, 103774	1.08	±	0.15	(*30*)	0.00	±	0.00	(*16*)
Tace	87	572, 109440	1.18	±	0.14	(*30*)	0.00	±	0.00	(*16*)
Tasp1	88	11588, 101158	1.02	±	0.14	(*30*)	0.00	±	0.00	(*16*)
tld	89	246, 106256	1.12	±	0.18	(*30*)	0.13	±	0.13	(*16*)
tok	90	101665, 245	1.16	±	0.21	(*30*)	0.00	±	0.00	(*16*)
Trol	7	24549, 110494	3.14	±	0.31	(*35*)	0.00	±	0.00	(*16*)
UQCR-C1	91	11056, 108539	1.12	±	0.22	(*30*)	0.00	±	0.00	(*16*)
UQCR-C2	92	11238, 108812	1.07	±	0.18	(*30*)	0.00	±	0.00	(*16*)
YME1L	93	2166, 102210	0.92	±	0.15	(*30*)	0.00	±	0.00	(*16*)

Table S2, related to STAR Methods. Genotypes of Experiments for the Study.
Complete genotypes of each experimental sample analyzed throughout the study, organized and denoted by figure panel.

Figure	Panel	Genotype	
1	C	+; +; +; +	
	D	w; +; $dfz2^{C1/Df}$; +	
	E	w; Mef2-GAL4 / UAS-dshDIX; +; +	
	G	Control	+; +; +; +
		dfz2	w; +; $dfz2^{C1/Df}$; +
		dfz2 + FL Fz2	w; Mef2-GAL4 / UAS-Fz2-FL; $dfz2^{C1/Df}$; +
		dfz2 + Fz2-C	w, UAS-myc-NLS-Fz2C; Mef2-GAL4 / +; $dfz2^{C1/Df}$; +
		dfz2 + ΔKTLES	w; Mef2-GAL4 / UAS-Fz2-DKTLES; $dfz2^{C1/Df}$; +
		dfz2 + ArmS10	w; Mef2-GAL4 / UAS-Arm^{S10}; $dfz2^{C1/Df}$; +
		Gal4 alone	w; Mef2-GAL4 / +; +; +
		Mef2 > Dsh^{DIX}	w; Mef2-GAL4 / UAS-dshDIX; +; +
2	A	+; +; +; +	
	C	w; Mef2-GAL4 / +; UAS-GFP-RNAi / +; +	
	D	w; Mef2-GAL4 / +; UAS-psn-IR-43082 / +; +	
	E	w; Mef2-GAL4 / +; UAS-nct-IR-JF02648 / +; +	
3	B	+; +; +; +	
	C	w; +; $psn^{143/C4}$; +	
	D	+; +; +; +	
	E	w; +; $nct^{A7/J2}$; +	
4	B, G	+; +; +; +	
	C, H	w; +; $psn^{143/C4}$; +	
	D, I	w; +; $nct^{A7/J2}$; +	
	E, J	Control	+; +; +; +
		psn	w; +; $psn^{143/C4}$; +
		psn + N	w; elav-GAL4 / UAS-psn-Nmyc; $psn^{143/C4}$; +
		psn + M	w; Mef2-GAL4 / UAS-psn-Nmyc; $psn^{143/C4}$; +
		psn RNAi Nerve	w; +; elav-GAL4 / UAS-psn-IR-43082; +
		psn RNAi Muscle	w; Mef2-GAL4 / +; UAS-psn-IR-43082 / +; +
		nct	w; +; $nct^{A7/J2}$; +
		nct + N	w; elav-GAL4 / +; nct^{A7} /nct ^{J2}, UAS-nct-myc; +
		nct + M	w; Mef2-GAL4 / +; nct^{A7} /nct ^{J2}, UAS-nct-myc; +
		nct RNAi Nerve	w; +; elav-GAL4 / UAS-nct-IR-JF02648; +
		nct RNAi Muscle	w; Mef2-GAL4 / +; UAS-nct-IR-JF02648 / +; +
	L, N, P	Control	+; +; +; +
		psn	w; +; $psn^{143/C4}$; +
		psn RNAi Nerve	w; +; elav-GAL4 / UAS-psn-IR-43082; +
		psn RNAi Muscle	w; Mef2-GAL4 / +; UAS-psn-IR-43082 / +; +
		nct	w; +; $nct^{A7/J2}$; +
		nct RNAi Nerve	w; +; elav-GAL4 / UAS-nct-IR-JF02648; +
		nct RNAi Muscle	w; Mef2-GAL4 / +; UAS-nct-IR-JF02648 / +; +
5	A	w; +; nct^{J2} / +; +	
	B	w; +; $dfz2^{C1}$ / +; +	
	C	w; +; nct^{J2} / $dfz2^{C1}$; +	
	D	Control	+; +; +; +
		psn -/+	w; +; psn^{143} / +; +
		nct -/+	w; +; nct^{J2} / +; +
		dfz2 -/+	w; +; $dfz2^{C1}$ / +; +
		psn -/+ nct -/+	w; +; psn^{143} / nct^{J2}; +
		psn -/+ dfz2 -/+	w; +; psn^{143} / $dfz2^{C1}$; +

		nct -/+ dfz2 -/+	*w; +; nct^{J2} / $dfz2^{C1}$; +*
		ten-a -/+	*Df(X)ten-a / +; +; +; +*
		ten-a -/+ nct -/+	*Df(X)ten-a / +; +; nct^{J2} / +; +*
		aph-1 -/- dfz2 -/-	*w; $aph\text{-}1^{D35/Df}$; $dfz2^{C1/Df}$; +*
	E – F	*w; UAS-Psn-Nmyc / UAS-Fz2-FLAG; Mef2-GAL4 / +; +*	
	G – H	*+; +; +; +*	
	I	*w; +; Mef2-GAL4 / UAS-nct-myc; +*	
	J – L	*Control*	*w; Mef2-GAL4 / UAS-Fz2-FLAG; +; +*
		β11 -/-	*w; imp-$β11^{70}$,UAS-Fz2-FLAG / Df(2R)Δm22; Mef2-GAL4 / +;*
		psn -/-	*w; Mef2-GAL4 / UAS-Fz2-FLAG; $psn^{143/C4}$; +*
		nct -/-	*w; Mef2-GAL4 / UAS-Fz2-FLAG; $nct^{A7/J2}$; +*
6	**B, G**	*+; +; +; +*	
	C, H	*w; Mef2-GAL4 / UAS-GFP-nls; psn^{143}; +*	
	D, I	*w, UAS-myc-NLS-Fz2C / + or Y; Mef2-GAL4 / +; psn^{143}; +*	
	E, J	*w; Mef2-GAL4 / UAS-GFP-nls; $nct^{A7/J2}$; +*	
	F, K	*w, UAS-myc-NLS-Fz2C / + or Y; Mef2-GAL4 / +; $nct^{A7/J2}$; +*	
	L-P	*Control*	*+; +; +; +*
		psn + GFP	*w; Mef2-GAL4 / UAS-GFP-nls; psn^{143}; +*
		psn + Fz2-C	*w, UAS-myc-NLS-Fz2C / + or Y; Mef2-GAL4 / +; psn^{143}; +*
		nct + GFP	*w; Mef2-GAL4 / UAS-GFP-nls; $nct^{A7/J2}$; +*
		nct + Fz2-C	*w, UAS-myc-NLS-Fz2C / + or Y; Mef2-GAL4 / +; $nct^{A7/J2}$; +*
7	**B, G**	*w^{1118}; +; +; +*	
	C, H	*w^{1118}; +; psn^{H185R}; +*	
	D, I	*w, UAS-myc-NLS-Fz2C / + or Y; Mef2-GAL4 / +; psn^{H185R}; +*	
	D, G	*w^{1118}; +; psn^{G228D}; +*	
	F, K	*w, UAS-myc-NLS-Fz2C / + or Y; Mef2-GAL4 / +; psn^{G228D}; +*	
	L – P	*Control*	*w^{1118}; +; +; +*
		psn^{H185R}	*w^{1118}; +; psn^{H185R}; +*
		psn^{H185R} + Fz2-C	*w, UAS-myc-NLS-Fz2C / + or Y; Mef2-GAL4 / +; psn^{H185R}; +*
		psn^{G228D}	*w^{1118}; +; psn^{G228D}; +*
		psn^{G228D} + Fz2-C	*w, UAS-myc-NLS-Fz2C / + or Y; Mef2-GAL4 / +; psn^{G228D}; +m*
S1	**A-B**	*w; UAS-psn-Nmyc / +; Mef2-GAL4 / +; +*	
	C-D	*w; +; Mef2-GAL4 / UAS-nct-myc; +*	
	E	*w; Or47b-GAL4, UAS-Brp-Short-mStraw / UAS-psn-Nmyc; +; +*	
	F	*w; UAS-Brp-Short-mStraw / +; Or67d-GAL4 / UAS-nct-myc; +*	
	G	*w; elav-GAL4 / UAS-psn-Nmyc; $psn^{143/C4}$; +*	
	H	*w; Mef2-GAL4 / UAS-psn-Nmyc; $psn^{143/C4}$; +*	
	I	*w; elav-GAL4 / +; nct^{A7} /nct ^{J2}, UAS-nct-myc; +*	
	J	*w; Mef2-GAL4 / +; nct^{A7} /nct ^{J2}, UAS-nct-myc; +*	
S2	**B, G**	*+; +; +; +*	
	C, H	*w; $aph\text{-}1^{D35/Df}$; +; +*	
	D, I	*w; $pen\text{-}2^{MI02639}$; +; +*	
	E, J	*Control*	*+; +; +; +*
		aph-1	*w; $aph\text{-}1^{D35/Df}$; +; +*
		aph-1 + N	*w; $aph\text{-}1^{D35/Df}$; Mef2-GAL4 / UAS-aph-1-V5; +*
		aph-1 + M	*w; $aph\text{-}1^{D35/Df}$; elav-GAL4 / UAS-aph-1-V5; +*
		aph-1 RNAi Nerve	*w; UAS-aph-1-IR-16820 / +; elav-GAL4 / +*
		aph-1 RNAi Muscle	*w; UAS-aph-1-IR-16820 / +; Mef2-GAL4 / +; +*
		pen-2	*w; $pen\text{-}2^{MI02639}$; +; +*
		pen-2 + N	*w; $pen\text{-}2^{MI02639}$; elav-GAL4 / UAS-pen-2-FLAG; +*
		pen-2 + M	*w; $pen\text{-}2^{MI02639}$; Mef2-GAL4 / UAS-pen-2-FLAG; +*
		pen-2 RNAi Nerve	*w; UAS-pen-2-IR-JF02608 / +; elav-GAL4 / +; +*
		pen-2 RNAi Muscle	*w; Mef2-GAL4 / UAS-pen-2-IR-JF02608; +; +*
	L-P	*Control*	*+; +; +; +*
		aph-1	*w; $aph\text{-}1^{D35/Df}$; +; +*
		aph-1 RNAi Nerve	*w; UAS-aph-1-IR-16820 / +; elav-GAL4 / +*

		aph-1 RNAi Muscle	*w; UAS-aph-1-IR-16820 / +; Mef2-GAL4 / +; +*
		pen-2	*w; pen-2^{MI02639}; +; +*
		pen-2 RNAi Nerve	*w; UAS-pen-2-IR-JF02608 / +; elav-GAL4 / +; +*
		pen-2 RNAi Muscle	*w; Mef2-GAL4 / UAS-pen-2-IR-JF02608; +; +*
S3	**A,F,K,P**	*+; +; +; +*	
	B,G,L,Q	*w; +; psn$^{143/C4}$; +*	
	C,H,M,R	*w; +; nct$^{A7/J2}$; +*	
	D,I,N,S	*w; aph-1$^{D35/Df}$; +; +*	
	E,J,O,T	*w; pen-2^{MI02639}; +; +*	
	U-Z	*Control*	*+; +; +; +*
		psn	*w; +; psn$^{143/C4}$; +*
		nct	*w; +; nct$^{A7/J2}$; +*
		aph-1	*w; aph-1$^{D35/Df}$; +; +*
		pen-2	*w; pen-2^{MI02639}; +; +*
S4	**A-B**	*+; +; +; +*	
	C	*w; +; psn$^{143/C4}$; +*	
	D	*Control*	*+; +; +; +*
		Psn	*w; +; psn$^{143/C4}$; +*
	E	*+; +; +; +*	
	F	*w, Appl^{d}; +; +; +*	
	G	*+; +; +; +*	
	H	*N^{ts1}; +; +; +*	
	I	*Control*	*+; +; +; +*
		Msk -/-	*w; +; msk^{5}; +*
		Muscle Kuz DN	*w; UAS-Kuz-DN / +; Mef2-GAL4 / +; +*
		Appl -/-	*w, Appl^{d}; +; +; +*
		Muscle mam IR	*w; Mef2-GAL4 / UAS-mam-IR-102091; +; +*
		Control HS	*+; +; +; +*
		N^{ts} HS	*N^{ts1}; +; +; +*
S5	**A-D,J-M**	*w; UAS-HA-Fz2-FLAG / +; 24B-GAL4 / UAS-Psn-myc; +*	
	E, H	*w; UAS-HA-Fz2-FLAG / +; 24B-GAL4 / +; +*	
	F, I	*w; +; 24B-GAL4 / UAS-Psn-myc; +*	
S6	**A, E**	*+; +; +; +*	
	B, F	*w; +; psn$^{143/C4}$; +*	
	C, G	*w; +; nct$^{A7/J2}$; +*	
	D, H	*Control*	*+; +; +; +*
		psn -/-	*w; +; psn$^{143/C4}$; +*
		nct -/-	*w; +; nct$^{A7/J2}$; +*
	I	*y, w; +; +; +*	
	J	*y, w; +; psn$^{143/C4}$; +*	
	K	*y, w; +; nct$^{J2/A7}$; +*	
	L	*Control*	*y, w; +; +; +*
		psn	*y, w; +; psn$^{143/C4}$; +*
		psn + N	*y, w; elav-GAL4 / UAS-psn-Nmyc; psn$^{143/C4}$; +*
		psn + M	*y, w; Mef2-GAL4 / UAS-psn-Nmyc; psn$^{143/C4}$; +*
		nct	*y, w; +; nct$^{A7/J2}$; +*
		nct + N	*y, w; elav-GAL4 / +; nct^{A7} /nct ^{J2}, UAS-nct-myc; +*
		nct + M	*y, w; Mef2-GAL4 / +; nct^{A7} /nct ^{J2}, UAS-nct-myc; +*
	N	*+; +; +; +*	
	O	*w; Mef2-GAL4 / UAS-Fz2+5AAAAA; dfz2$^{C1/Df}$; +*	
	P	*Control*	*+; +; +; +*
		dfz2	*w; +; dfz2$^{C1/Df}$; +*
		Dfz2 + 5A	*w; Mef2-GAL4 / UAS-Fz2+AAAAA; dfz2$^{C1/Df}$; +*
S7	**A**	*w, UAS-Dcr2 / Y; UAS-Brp-Short-Straw / +; Or67d-GAL4 / +; +*	
	B	*w, UAS-Dcr2 / Y; UAS-Brp-Short-Straw / +; Or67d-GAL4 / UAS-psn-IR-43082; +*	
	C	*w, UAS-Dcr2 / Y; UAS-Brp-Short-Straw / +; Or67d-GAL4 / UAS-nct-IR-JF02648; +*	
	D	*w, UAS-Dcr2 / Y; UAS-Brp-Short-Straw / UAS-aph-1-IR-16820; Or67d-GAL4 / +; +*	
	E	*w, UAS-Dcr2 / Y; +; Or67d-GAL4, UAS-mCD8-GFP / +; +*	
	F	*w, UAS-Dcr2 / Y; +; Or67d-GAL4, UAS-mCD8-GFP / UAS-psn-IR-43082; +*	

	G	*w, UAS-Dcr2 / Y; +; Or67d-GAL4, UAS-mCD8-GFP / UAS-nct-IR-JF02648; +*	
	H	*w, UAS-Dcr2 / Y; UAS-aph-1-IR-16820 / +; Or67d-GAL4, UAS-mCD8-GFP / +; +*	
	I	*Control*	*w, UAS-Dcr2 / Y; UAS-Brp-Short-Straw / +; Or67d-GAL4 / +; +*
		psn RNAi	*w, UAS-Dcr2 / Y; UAS-Brp-Short-Straw / +; Or67d-GAL4 / UAS-psn-IR-43082; +*
		nct RNAi	*w, UAS-Dcr2 / Y; UAS-Brp-Short-Straw / +; Or67d-GAL4 / UAS-nct-IR-JF02648;*
		aph-1 RNAi	*w, UAS-Dcr2 / Y; UAS-Brp-Short-Straw / UAS-aph-1-IR-16820; Or67d-GAL4 / +;*
	J	*Control*	*w, UAS-Dcr2 / w; UAS-Brp-Short-Straw / +; Or67d-GAL4 / +; +*
		psn RNAi	*w, UAS-Dcr2 / w; UAS-Brp-Short-Straw / +; Or67d-GAL4 / UAS-psn-IR-43082; +*
		nct RNAi	*w, UAS-Dcr2 / w; UAS-Brp-Short-Straw / +; Or67d-GAL4 / UAS-nct-IR-JF02648;*
		aph-1 RNAi	*w, UAS-Dcr2 / Y; UAS-Brp-Short-Straw / UAS-aph-1-IR-16820; Or67d-GAL4 / +;*
	K	*Control*	*w, UAS-Dcr2 / w; +; Or67d-GAL4, UAS-mCD8-GFP / +; +*
		psn RNAi	*w, UAS-Dcr2 / Y; +; Or67d-GAL4, UAS-mCD8-GFP / UAS-psn-IR-43082; +*
		nct RNAi	*w, UAS-Dcr2 / Y; +; Or67d-GAL4, UAS-mCD8-GFP / UAS-nct-IR-JF02648; +*
		aph-1 RNAi	*w, UAS-Dcr2 / Y; UAS-aph-1-IR-16820 / +; Or67d-GAL4, UAS-mCD8-GFP / +; +*
	L	*Control*	*w, UAS-Dcr2 / w; +; Or67d-GAL4, UAS-mCD8-GFP / +; +*
		psn RNAi	*w, UAS-Dcr2 / w; +; Or67d-GAL4, UAS-mCD8-GFP / UAS-psn-IR-43082; +*
		nct RNAi	*w, UAS-Dcr2 / w; +; Or67d-GAL4, UAS-mCD8-GFP / UAS-nct-IR-JF02648; +*
		aph-1 RNAi	*w, UAS-Dcr2 / w; UAS-aph-1-IR-16820 / +; Or67d-GAL4, UAS-mCD8-GFP / +; +*